Evaluation of Formalin Fixation for Tissue Biopsies Using Shear Wave Laser Speckle Imaging System

SANIEL D. LIM[ID]**[1,2,3], QIXUAN HUANG**[ID]**[2,4], AND ERIC J. SEIBEL[1,2,3]**

[1]Mechanical Engineering Department, University of Washington, Seattle, WA 98195, USA
[2]Human Photonics Lab, University of Washington, Seattle, WA 98195, USA
[3]University of Washington, Seattle, WA 98195, USA
[4]Computer Science Department, Georgia Institute of Technology, Atlanta, GA 30332, USA

CORRESPONDING AUTHOR: E. J. SEIBEL (eseibel@uw.edu)

ABSTRACT Chemical fixation is the slowest and often the most uncontrolled step in the multi-step process of preparing tissue for histopathology. In order to reduce the time from taking a core needle biopsy to making a diagnosis, a new approach is proposed that optically monitors the common formalin fixation process. A low-cost and highly-sensitive laser speckle imaging technique is developed to measure shear wave velocity in a biospecimen as small as 0.5 mm in thickness submerged in millifluidic channels. Shear wave velocity, which is the indicator of tissue mechanical property and induced by piezoelectric-actuation, was monitored using gelatin phantom and chicken breast during fixation, as well as post-fixed liver and colon tissues from human. Fixation levels in terms of shear wave velocity increased by approximately 271.0% and 130.8% in gelatin phantom and chicken breast, respectively, before reaching the plateaus at 10.91 m/s and 7.88 m/s. Within these small specimens, the plateaus levels and times varied with location of measurement, and between gelatin and chicken breast. This optical-based approach demonstrates the feasibility of fine-tuning preanalytical variables, such as fixation time, for a rapid and accurate histopathological evaluation; provides a quality metric during the tissue preparation protocol performed in most pathology labs; and introduces the millifluidic chamber that can be engineered to be a future disposable device that automates biopsy processing and imaging.

INDEX TERMS Biomedical optical sensing, elastography monitoring, tissue mechanics, histology biopsy preparation.

I. INTRODUCTION

In medical practice, multiple trends are modernizing pathology, such as (1) increasing reliance on biopsy tissue processing in disease diagnosis which also influences therapeutic approaches, (2) obtaining biopsies from more minimally invasive procedures like needles, and (3) providing more rapid and less destructive tissue analysis of these smaller specimens from coring needles.

Histopathologic study of clinical tissue biopsies from suspicious lesions is considered the gold standard to identify and confirm disease diagnosis (e.g., cancer). Regardless of the size or type, currently all tissue biopsies are chemically-fixed to satisfy three primary criteria: specimen handling,

absorptive/fluorescent staining, and antigen retrieval for immunohistochemical analyses. 10% neutral buffered formalin (NBF) has been most commonly used and best characterized in the pathology laboratories for more than 100 years [1], [2]. Formalin fixation is the slowest step in biospecimen preparation process in which formalin fixative penetrates tissue relatively fast due to a small molecule of formaldehyde, however, the binding (covalent cross-linking) process between proteins by formaldehyde is quite slow [3]. Without clinical complexity, the speed of formalin fixation is generally recognized at 0.5 - 1.0 mm/hour, which is oversimplified. For example, there are recommended fixation times for human tissues, such as 6 to 72 hours of fixation for

estrogen receptor (ER), progesterone receptor (PgR), and human epidermal growth factor receptor 2 (HER2) testing for breast cancer [4], and more than 8 hours for quantum dot (QD) in situ hybridization (ISH) in prostate needle biopsy [5]. However, in most cases, pathology laboratories develop the effective preanalytical factors in tissue handling, such as fixation time, through empirical approach based on their infrastructure, tissue geometry, and target biomarkers, presumably because of a lack of standardized fixation parameters. Some experts present conflicting results to the consensus recommendations [6]–[8] and even claim that those consensus recommendations describe largely "faith-based" exercises, and not based on the scientific evidence [9]. When fixation is not properly completed, mostly underfixed, the tissue cannot be restored, and the results of histological and molecular pathological diagnosis can be erroneous, e.g., tissue distortion, poor quality of staining, while over-fixation can be partially reversed by antigen retrieval [5], [10]–[12]. In addition, more efforts to understand the preanalytical variables, especially fixation approach, in conventional biospecimen process are being made as cancer immunotherapy techniques are being translated into the clinic, which requires the high-quality nucleic acids for molecular diagnosis [13]–[15].

Minimally-invasive biopsy, such as core needle biopsy (CNB), is becoming more common as a tissue sampling method in cancer management because of the great benefits of being cost-effective, less painful, easier sampling, and lower postoperative morbidity compared to a surgical biopsy [16]–[18]. Each year in the United States, several million needle biopsies from various organs are procured: 1.6 million breast biopsies [17], 1 million prostate biopsies (only in the Medicare population) [19], plus lung biopsies, liver biopsies, pancreatic biopsies, etc. Now, minimally invasive CNB for breast tissue diagnosis is the "optimal initial tissue-acquisition method and the procedure of choice for image-detected breast abnormalities" and has been advocated to become the standard of care [20].

The small size of CNB makes the tissue specimen valuable because of tissue scarcity for diagnostics, and also chemical processing times are reduced with such small volumes (typically $10 - 40 \, mm^3$). Since chemical fixation is the slowest step in the established process of histopathology, speeding up this process has been the focus of numerous studies. One approach is enhancing the fixation process with or without NBF, such as rapid two-temperature fixation [21], elevated pressure fixation [22], ultrasound-facilitated fixation [23], microwave fixation [24]. Alternatively, there have been persistent studies on alcohol-based fixatives, which offers faster fixation and longer preservation of protein, DNA, and RNA while having a similar histomorphology by NBF [25]–[28]. Implementation of all these different techniques requires a highly flexible laboratory environment, while manually handling CNBs is tedious and overnight tissue batch preparation

with a tissue processor is needlessly slow. Instead, the small specimen size lends itself well to an enlarged version of microfluidics or millifluidics where Lab-on-a-Chip technologies can process small biospecimens. This novel millifluidic device, which is under development in our lab [29]–[31], may aid clinicians in the rapid assessment of CNBs. Once imaged within the device, the specimen may be seamlessly passed into the standard pathology workflow and conventional histopathological evaluation.

Thus, the previous listed three multiple trends modernizing pathology may soon require the development of process control of the CNB sample preparation, which would include real-time monitoring of chemical fixation. There has been a study to quantitatively monitor the fixative diffusion using an ultrasonic time-of-flight technique [32]. However, the fixative diffusion is not correlated to the structural modification by fixation, which cannot be solely evaluated by compressional wave transport, especially in two-phase (liquid-solid) interfaces. In contrast, shear wave, which can only propagate in solids, is feasible to detect the real-time structural changes of the biospecimen while submerged in fixative. For the shear wave propagation, laser speckle imaging (LSI) is a highly sensitive and relatively low-cost configuration without experimental complexity compared to other imaging modalities (e.g., ultrasound, OCT and MRI). Furthermore, LSI can be used on a small CNB sample in a millifluidic chamber.

In this paper, we propose the shear wave laser speckle imaging (SW-LSI) configuration to measure the SW velocity (SWV) of a CNB-sized specimen in NBF-filled millifluidic channels, by which the dimensional and temporal changes of the fixation level were evaluated in terms of the stiffness indicator, shear wave. The approach uses non-destructive optical light scattering which can be conducted on these small specimens within a small millifluidic chamber or channel. Low cost and portability are also requirements since these fixation monitors are designed to be ultimately used at the point-of-care. In this preliminary study, the SWV at different depths of a sub-centimeter-scale submerged gelatin phantom and chicken breast sample are measured to quantitatively track the biopsy-sized specimen's fixation level during formalin-fixation in millifluidic channels. The results of SW-LSI measurement in biological tissue, including any animal tissue, is presented for the first time. In addition, monitoring the formalin fixation using SW-LSI, to the best of our knowledge, has not been reported previously. The ancillary measurements of fully fixed human liver and colon biopsy are also added to the comprehensive results from 6% gelatin phantom and chicken breast. In conclusion, we propose that this noninvasive fixation monitoring system helps to eliminate redundant tissue preparation time in avoiding underfixation, eventually reduce the labor costs of manual processing, and have the potential to finely engineer fixation protocols for tissue size, type, and specific molecular biomarkers as well as other fixatives.

II. MATERIALS AND METHODS

A. OPTICAL-BASED APPARATUS FOR SHEAR WAVE VELOCITY MEASUREMENT

Elasticity measurement can be achieved through two methods; strain ratio and acoustic wave velocity measurement. The strain ratio measurement under static or dynamic compression is a simple and straightforward method. However, this technique is not able to measure Young's modulus quantitatively because the applied local stress is difficult to measure. The properties of acoustic waves can also be used for elasticity. Wave propagation speed is characterized by the acoustic impedance which depends on the mass and elasticity of tissue. The speed of compression wave is determined by the bulk modulus (the inverse of the compressibility) and density of both solid and fluid media. In contrast, the speed of shear wave is dependent on the shear modulus and density of a solid. Therefore, the measurement of shear wave is more suitable to determine the mechanical property change of tissue, ignoring the effect of the proportions of interstitial fluid and other solutions, i.e., fixative. Another advantage of shear wave is that the broad range of its velocity compared to that of compressional wave which differs less than one-thousandth of the velocity in different tissue types [33]. The shear wave is expressed by Newton-Laplace equation in terms of the shear modulus and density of a medium; $v_s = \sqrt{(G/\rho)}$, where G is shear modulus, v_s is shear wave speed, and ρ is solid's density.

LSI detects and evaluates dynamic motions in a scattering medium using the spatiotemporal change of local 2D speckle patterns [34]–[36]. Speckle pattern is the interference pattern formed by the illumination of scattering particles, and the series of the temporal speckle patterns are similar in appearance to the video of fast-moving objects captured by a camera. And those movements (i.e., shear wave) are shown as the temporal change of local speckle patterns with a short camera exposure time or the local blurring with long exposure time. The speckle pattern series, therefore, reveal the spatiotemporal distribution of shear wave. High-resolution speckle patterns can be monitored through magnification (i.e., a 5X objective) and at substantially higher SNRs as pixel (px) sizes for machine vision cameras are continuously trending to smaller sizes (7.4 μm). LSI systems are additionally simple to set up as a benchtop apparatus (Fig. 1).

B. SAMPLE PREPARATION

This formalin fixation study was divided into two parts: a dimensional study and temporal study. The dimensional study aimed to evaluate the fixation level change at different depths in a thick specimen (width = 15 mm). In the temporal study, the average fixation level change in a thin specimen (width = 1.5 mm) was investigated over time. Gelatin phantom used in both studies was not only chosen for a rapid and easy way to control the phantom characteristics, but also to mimic the chemical fixation process in soft tissue by formalin [37]. The gelatin phantoms were fabricated with the gelatin
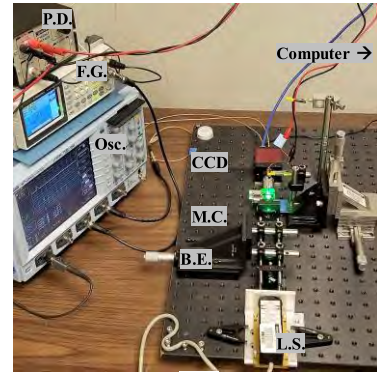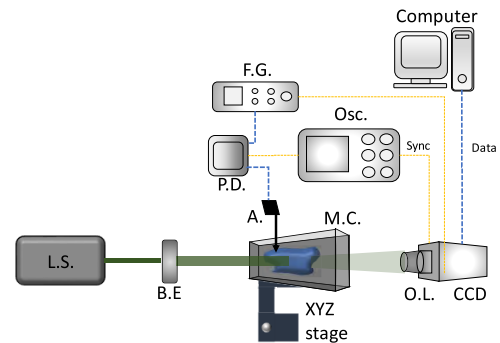
FIGURE 1. (a) An experimental apparatus (b) A schematic of experimental setup on left. L.S.: laser source, B.E.: beam expander, M.C.:milifludic chamber, O.L.:objective lens, A.:actuator, P.D.:piezo driver, F.G.:function generator, Osc.:oscilloscope.

powder (Sigma-Aldrich, 300 Bloom) at the mass concentration of 6% and Titanium Oxide (US Research Nanomaterials, Inc., TiO2 18nm) at the mass concentration of 0.3% to enhance optical scattering. In addition, fresh chicken breast was prepared to compare the fixation behavior with gelatin phantom. The human liver and colon tissue after prolonged formalin fixation were also prepared to benchmark for clinical translation.

1) DIMENSIONAL STUDY

Gelatin phantom and chicken breast cut in a cube shape, at 15mm×15mm×15mm, were used during formalin fixation and later sliced into a biopsy sample for imaging. A single specimen cube was required for every hour of image acquisition, e.g., fresh, 1 hour, 2 hours, and so on. The prepared cubic samples were immersed within a 15 times greater volume of NBF. Each hour during fixation, one cube was sectioned into CNB cross-sectional size, approximately 1.5mm×2mm×2mm, for three different depth points of interest (i.e., 1.5mm, 4.5mm, and 7.5mm in depth from surface) and placed in a custom-designed water-filled open-top cuvette (Fig. 2). The sliced specimen was completely submerged, and the focal plane of the sensor was placed to the middle of the slice, which was the specified depth from the surface of the block.
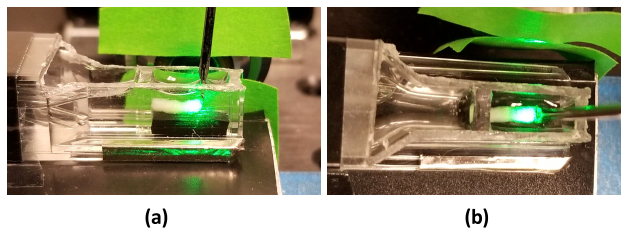
FIGURE 2. Chicken breast tissue located in a cuvette channel filled with formalin. (a) side view and (b) top view.

FIGURE 3. (a) A grid of reference and target nodes. (b) Example correlation coefficient signals of fresh 6% gelatin over time at the reference and target (every 10th) nodes averaged along the vertical dotted box shown in (a).

2) TEMPORAL STUDY

To evaluate the mechanical property change of a 2mm biopsy-sized specimen by NBF, SWV measurement was conducted within short time intervals (10-15 minutes) over 3 hours (up to 5 hours with a longer time interval, around 30 minutes) for gelatin and 4 hours for chicken breast. The specimen was not moved during the entire experiment after it was positioned in the millifluidic channel. The channel holds more than 20 times more volume of NBF than the specimen.

3) HUMAN TISSUE MEASUREMENT

Human liver and colon extra tissue samples were also acquired from University of Washington Northwest Biotrust. IRB approval was already obtained by the principal investigators (Eric Seibel and Rodney Schmidt, retired Pathologist). The tissues, in about 10 mm^3 block size, were kept in NBF more than three months, which were considered as prolonged fixation. Both tissue types were cut down to 0.5mm and 1mm in thickness for liver and colon tissues to allow for strong optical scattering. Positioning and measuring protocols were the same as above.

C. SYSTEM OPERATION

A 532nm 10mW laser (B&W Tek, BWN-532-10E) was expanded to a 3mm-diameter collimated beam and transmitted through a tissue biopsy sample orthogonal to the propagation direction of the shear wave, thus producing a speckle pattern image. Polarizing and neutral density filters were introduced after the beam expander to adjust speckle pattern intensity variation based on specimen thickness and camera exposure time (Fig. 1). A machine vision camera (Allied Vision, Prosilica GE1650, 1.9MP CCD) was precisely positioned opposite the laser beam to capture the speckle pattern over time. Phantom or tissue in a millifluidic channel attached to an XYZ-translation stage was located between the laser and camera. The dimension of the open-top millifluidic channel is 4mm × 5mm × 15mm (width × height × length), allowing placement of thick CNBs up to 9-gauge needle size. Disposable cuvette is customized for millifluidic channels because of low cost and easy reproduction, however, glass-based channels can also be used. A flat-headed needle tip of a stack piezoelectric actuator (STEMiNC, SMPAK15553D4, 3 × 3 × 5mm, 0.15uF) provided vertical force to the sample in the millifluidic channels. The displacement of the force
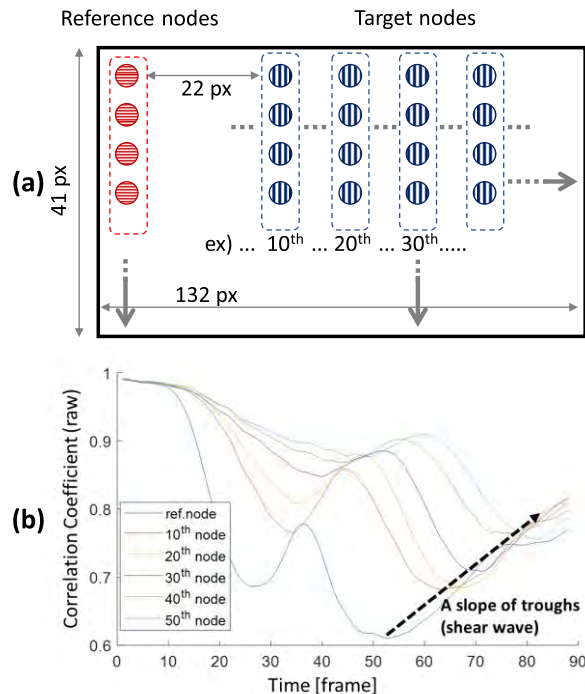
was set to 0.5 μm, and a single cycle of 1000 Hz sinusoidal signal was applied. The laser speckle pattern was recorded by the camera with a magnification of 5 power (5×) through an objective lens. The minimum speckle size (S) is estimated by the relationship, $S = 2.44 \frac{(1+M) \times \frac{f}{\#}}{\lambda}$, where λ is a laser wavelength, M is the imaging magnification, f/# is the f-number of the imaging system. And, our system has a minimum speckle size of 38.5 μm and equivalent to 5.2 pixels (N = 5.2). The spatially oversampled speckle patterns have slightly better resolution than the Nyquist sampling criteria, N = 2 [38].

Once the specimen was inserted in the millifluidic channel, the field of view (FOV) of the camera and the contact position of the piezoelectric actuator (piezo) tip on the specimen contact were adjusted to locate the point of piezo force on the top side edge of the FOV to maximize the distance of shear wave propagation within FOV (d = 1.8 mm). And the midplane of the specimen, the identical plane of the piezo tip, was then focused by the objective lens and sensor. MATLAB image acquisition toolbox was used to acquire image data and operate the camera, which was synchronized with a piezo amplifier (A.A. Lab Systems, A-301HS), a function generator (GW Instek, AFG-2225), and an oscilloscope (LeCroy, LT374M).

D. DATA ACQUISITION

The region of interest for the CCD sensor was cropped to 400 px × 1200 px for fast data acquisition which increased the frame rate from 30 to 50 frames/second. The 12-bit
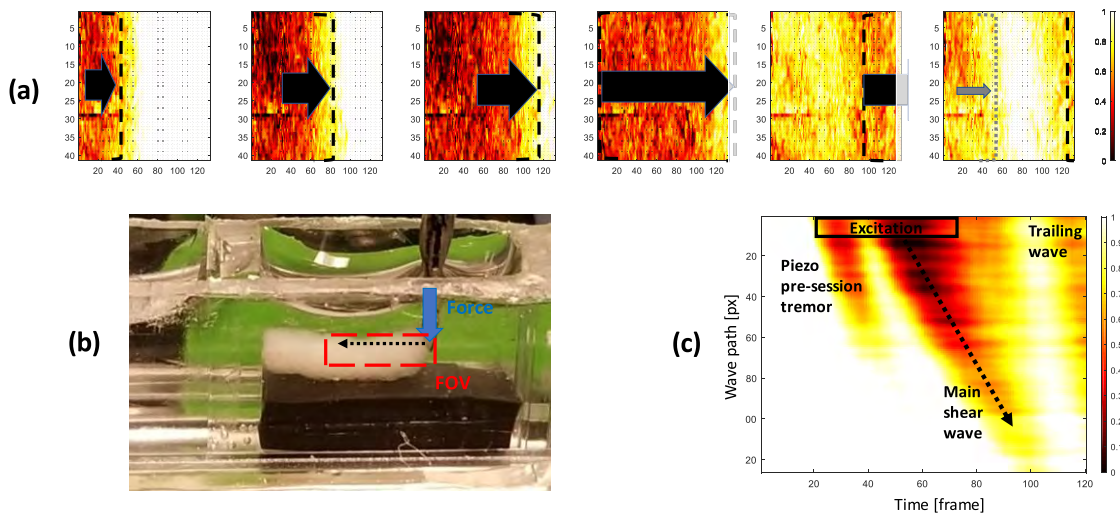
FIGURE 4. (a) Example shear wave propagation in speckle correlation maps (41px × 132px) at 0μs, 172.6μs, 345.3μs, 517.9μs, 690.9μs, 863.2μs, respectively. Low values of correlation coefficient indicate the shear wave (black arrow) and the last screen shows the following wave (small gray arrow). (b) Field of view (red box) in a chicken breast specimen. Shear wave propagation direction (black arrow) from the piezo excitation (blue arrow). (c) Spatiotemporal map of the specimen same location of FOV in in (b). The excitation duration was 1ms (single pulse at 1kHz) as shown with the black box (1ms is equivalent to 50 frames at the sampling frequency of 50kHz). The weak waves before and after the shear wave are presumably due to the inertial mass of the piezo actuator and tip.

sampling depth of an analog to digital converter was selected to record over 8-bit to increase the sensitivity of speckle pattern imaging as the speckle images suffer from significant noise. Due to the restriction of the frame rate, sequential equivalent-time sampling was employed to increase the effective camera frame rate [39]. For instance, when the camera frame rate was set to 50.00 Hz, the excitation pulse was repeated at the slightly faster frequency, 50.05005 Hz (period = 19.98 ms). The incremental time delay between camera frame rate and mechanical excitation frequency was registered in every camera frame such that the effective frame rate of the system corresponded to 50.00×10^3 frames/second.

E. IMAGE AND SIGNAL PROCESSING

1) IMAGE PROCESSING

The local speckle change, or disturbance, due to shear wave propagation was visualized after computing speckle correlation. A unique speckle pattern in a 2D kernel was compared to the one at the same location in later frame interval, returning correlation values. 2D kernel size was 22 px ×11 px of which twice larger size in the vertical direction parallel to the piezo tip alignment was specified to better detect the up and down movement of shear wave. The correlation computation for 2D kernel was conducted on a uniformly spaced grid over an image, a node per 9 pixels, to decrease the computation time down to 45 seconds per a single set of 600 speckle images (Intel i7-4820K, parallel computing), hence, the pixel dimension of the correlation coefficient images was decreased to 41 px ×132 px (Fig. 3(a)). And to increase signal-to-noise ratio by rejecting background low-frequency noise, the

reference image of the speckle kernels kept a constant time interval (i.e., 100 frames) from the processing image frame. The set of correlation coefficient images then visualized shear wave propagation as shown in Fig. 4(a). In Fig. 4(c), a spatiotemporal plot from the correlation images by averaging in the vertical direction and the actual location and the direction of the shear wave were shown in Fig. 4(b). The slope of the shear wave, the dotted arrow in Fig. 4(c), represents the SWV (SWV $=\frac{dx}{dt}$).

2) SIGNAL PROCESSING

Time to peak (TTP) cross-correlation method is the most common approach with shear wave elasticity imaging [40]. We implemented the TTP method with multiple improvements to suppress very strong noise in laser speckle images from unevenly-accumulated laser scattering, sample inhomogeneity, viscoelasticity, and external vibrations. Shear wave estimation was calculated between the excitation region and detection region. The minimum distance between regions was set to 22 px in the correlation map (equivalent to 200 px in a raw speckle image) to avoid significant error resulting from cross-correlation within a very short interval of time and distance. The detection region was not selected within a specific distance from the excitation area but chosen in multiple locations with gradual distances from the excitation to apply a linear fitting over the image. Fig. 3(a) shows the diagram of the node grid. The main shear wave area, the most decorrelated area, was zoomed in for further signal processing. In Fig. 3(b), the signals along the wave propagating direction were plotted; the deep troughs represented the main shear wave and the time delays were shown at

TABLE 1. Summary of SWV in the dimensional study: 6%(w/w) Gelatin and Chicken breast.

|		SWV ± SD [m/s]							
		Fixation hours							
Specimen	Depth	0	1	2	3	4	5	9	10
6% Gelatin	1.5mm	1.62±0.04	4.63±0.18	6.29±0.19	7.55±0.35	7.67±0.39	8.78±0.42	9.21±0.42	9.81±0.46
	4.5mm	1.62±0.04	2.14±0.03	3.03±0.09	4.25±0.19	5.75±0.28	6.09±0.34	6.43±0.17	6.77±0.08
	7.5mm	1.62±0.04	1.67±0.06	2.03±0.07	2.47±0.12	4.36±0.19	4.39±0.15	5.10±0.27	5.36±0.15
Chicken Breast	1.5mm	5.50±0.17	8.94±0.31	10.32±0.28	9.59±0.29	10.55±0.32	9.25±0.22	-	-
	4.5mm	5.50±0.17	7.00±0.25	8.18±0.25	8.27±0.37	10.67±0.30	9.62±0.25	-	-
	7.5mm	5.50±0.17	5.96±0.14	5.80±0.23	7.51±0.26	9.64±0.37	10.17±0.26	-	-
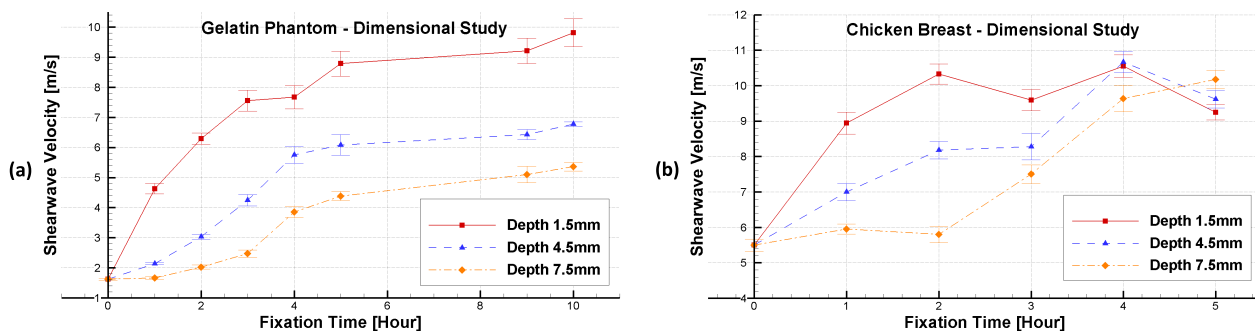
FIGURE 5. Change of shear wave in the dimensional study. The error bars represent the plus and minus of the standard deviation from the mean SWV. (a) 6% gelatin phantom (b) chicken breast
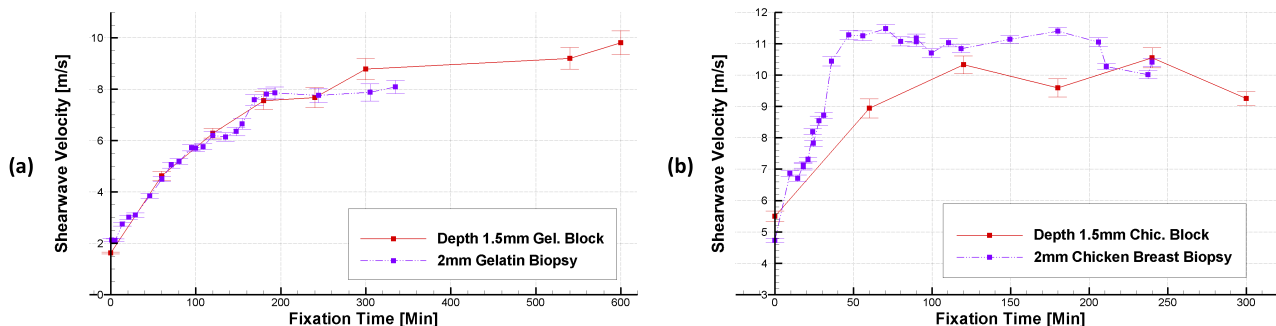

FIGURE 6. Change of shear wave in the 2mm biopsy study (Purple point and line). The error bars represent the plus and minus of the standard deviation from the mean SWV. (a) 6% gelatin phantom (b) chicken breast. The SWVs of the outer area (1.5mm depth from the sample block surface) in dimensional study are overlaid (Red point and line).

every 10th node from the reference location. Instead of simply estimating TOF of wavefront of the peak, we used the cross-correlation between reference and target signals so that the signal distortion due to wave attenuation and dispersion effects was partially compensated. The signals at nodes were normalized and processed with a low-pass (<20kHz) and high-pass (>100Hz) filters to reject other vibrations except for excitation wave. The correlation process also made use of a zero-phase crossing (ZPC) technique which overcomes the limit of the discrete temporal resolution, which was a frame. From the result of time delay and distance with the node grid, a straight-line robust regression with the bisquare weighting function determines the shear wave group velocity excluding measurement errors or significant outliers.

III. RESULTS
A. DIMENSIONAL STUDY
The spatiotemporal change of SWV in 6% gelatin phantom and chicken breast under formalin fixation are presented in Table 1 and Fig. 5. The SWV prior to fixation was measured once for all depths. During formalin fixation of gelatin phantom, the SWV increases rapidly during the first 3 hours at 1.5mm depth before the stiffening rate slows down. The stiffening at 4.5mm and 7.5mm depths are slower than the outer area, but they also become sluggish after 4 hours of fixation. The SWV of chicken breast shows similar stiffening behavior up to 3 hours fixation, however the SWVs at all depths reach the equivalent level of the plateau.

B. 2MM BIOPSY TEMPORAL STUDY

Fig. 6 shows the change of the SWV over time in 2mm size of 6% gelatin and chicken breast. The changes in SWV with gelatin phantom shows the gradual increase up to 3 hours of fixation, while the chicken breast specimen rapidly stiffens within an hour and becomes stationary. A small drop, about 10%, is observed in the chicken breast case as it is also shown in the dimensional study.
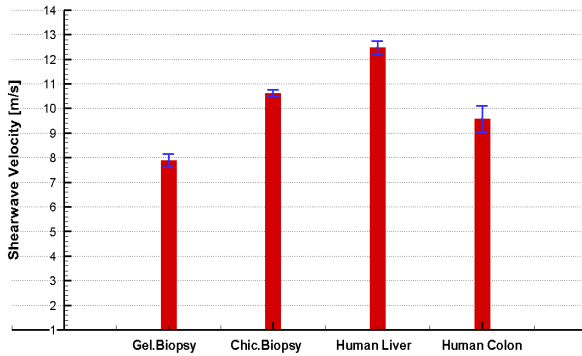

FIGURE 7. Prolonged-fixed human tissue measurements compared to fixed 6% gelatin and chicken breast biopsies.

C. FIXED HUMAN TISSUE MEASUREMENTS

Prolonged-fixed (more than 3 months) human normal liver and colon tissue were also observed in our setup. Fig. 7 displays the SWVs of 3-hour fixed 2mm gelatin and chicken breast in addition to fixed human liver and colon. Human liver and colon tissue yield 12.5 ± 0.27 m/s and 9.6 ± 0.53 m/s of SWV, respectively.

IV. DISCUSSION

The SWV changes of gelatin phantom and chicken breast during formalin fixation were investigated using the LSI system in this study. The specimen's thicknesses ranged from sub-millimeter using human tissue to two millimeters using chicken breast and 1 to 4 mm using tissue-mimicking phantoms. The use of small specimen size is unlike other LSI studies [34], [41], [42], where the size of the tissue-mimicking phantom ranged from 12 mm to 40 mm. In our LSI visible light system, the image processing for SWV measurement requires a minimum FOV of 150 μm $\times$ 450 μm (height $\times$ length), which sets the minimal specimen thickness. Thus, all CNBs and possibly even fragmented CNBs can be monitored for fixation within a millifluidic channel of diameter 1-5 mm.

The SWV of 6% gelatin phantom is in good agreement other gelatin studies; SWV at 2 ± 0.5 m/s estimated by Orescanin and Insana in 2010 [43] is within 22% error of our results (averaged SWV of fresh gelatin), and the SWV at 1.63 m/s reported by Manapuram et al., in 2012 [44] is within 0.6% of our results. In addition, according to the extensive literature review by Sarvazyan et al. in 2013 [33], various shear wave velocities in human breadst, liver, kidney, lung, and spleen are within a range of 0.85 m/s and 3.54 m/s,

which fall into the SWV range of fresh or fixed 6% gelatin. There is little stiffness information for fixed human tissues, however, animal tissues (chicken breast, cartilage, and tendon, and porcine fat and liver) are known to be stiffened approximately by 50-170 % [45], which are also within our SWV measurement range, 2-13 m/s.

Chemical fixation (covalent crosslinking) begins at the exposed surfaces where the formalin is diffusing through. However, the fixation levels inside the specimen were varied by the different specimen structure; homogeneous (6% gelatin) and heterogeneous (chicken breast). Fig. 8 shows the graphical illustration of the fixation level comparison between isotropic and anisotropic specimens, which is discussed in the following section.
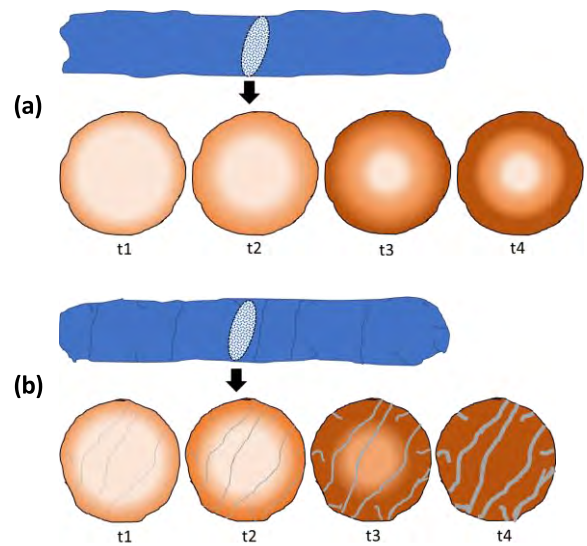

FIGURE 8. Illustration of fixation progress in (a) an isotropic model for 6% gelatin and (b) an anisotropic model for chicken breast. Gradient color represents the level of fixation and fixation time elapses from t1 to t4. The heterogeneous divisions, such as delamination and cracks, are displayed in (b), widening over time. For visual purpose, three discrete annular regions for fixation level are depicted in the cross-sectional area of CNBs.

In the dimensional study of the gelatin phantom (Fig. 5(a) and Fig. 8(a)), the fixation rates which is the slopes of SWV increases were differentiated at each depth as the supply of formalin was controlled by the fixation process. As the outer area contacted with sufficient formalin is stiffened rapidly and acts as a barrier to subsequent inward formalin diffusion [46]. The fixation process in the inner core of the sample is then gradually restricted by the formaldehyde supply. Therefore, the SWV plateau of inner sides was reached at different values from the outside. Because the long-term fixation of gelatin phantom with a small portion (about 0.4% of formalin mass fraction) showed that the stiffness of the gelatin took about 100 days to reach its equilibrium [37], it is not yet clear whether the 6% gelatin block becomes more stiffened after this sufficient exposure to formalin. However, the smooth slope change of SWV up to its plateau was demonstrated

and any significant hardening was not shown after 10 hours. It should be also noted that the similar trend, being plateaued after constant increments, of clinical Q score of estrogen receptor over the mean fixation times for human breast CNB was presented in Goldstein *et al.* study [10]. Chicken breast in Fig. 5(b), however, exhibited the dissimilar behavior that SWVs at three different depths reached the similar value (9.47 ± 0.97 m/s) after 4 hours formalin fixation. Although it is difficult to interpret too much from these preliminary results, the structural anisotropy in chicken breast muscle tissue likely facilitates the inward formalin diffusion, resulting in more rapid and spatially uniform SWV, see Fig. 8(b). The structure of fresh chicken breast looked heterogeneously stratified but dense and well-bonded, however, those layers become loosened as formalin is introduced after about an hour. For that reason, the delaminated chicken breast layers appear to allow formalin to flow inside the tissue resulting in the uniformly fixed condition at t4 (Fig. 8(b)). These observations may also explain the small (< 10%) SWV fluctuation once the SWV was plateaued, which was not shown in the gelatin measurements.

The results from the temporal study with 2mm-biopsy sized specimens in Fig. 6 (purple lines) also showed graphical correspondence to the results of the outer surface of the large block in Fig. 5, which is overlaid in Fig. 6 (red lines). Although the gelatin phantoms correspond very well between two measurements, the chicken breast shows a large discrepancy (2.2 times faster rate increase of SWV in 2mm biopsy) during the first hour of fixation. However, this could be explained by the structure of chicken breast as explained above. In addition, although the cautious handling with a fresh razor blade or sharp scalpel was necessary to avoid the coarse roughness or torn-like surfaces of raw tissue specimens, the preparation of the 2mm-sized raw chicken breast specimen was challenging which causes damage on the small sample, while preparing the larger fresh tissue block required much less effort, causing less damage.

In the human fixed tissue measurement (Fig. 7), fully-fixed human liver and colon samples were measured with our apparatus. The fixed liver specimen showed the strong scattering at 532nm laser wavelength. So, the thickness for measurements was adjusted down to 0.5 mm until the current apparatus was able to acquire useful speckle pattern images (SNR > 2.6, in speckle correlation images). In contrast, the colon specimen in 2mm thickness was measured at the similar scattering of our 6% gelatin with TiO^2. Although relative fixation level was not measured, these pilot data suggest the feasibility of our shear wave LSI setup for human organ tissues.

It should be noted that the SWV measurement offers a quantitative evaluation of specimen's mechanical property, in which SWV is proportional to the square root of shear modulus (or elastic modulus) assuming a linear elastic behavior and small deformations. Although soft tissue is generally viscoelastic, this assumption is broadly accepted in the elastography fields [47] for short response time at small displacements. Because of its simple and straightforward unit conversion, our results are presented with SWV in [m/s] instead of shear or elastic modulus in [kPa].

Throughout this report, we simply employ the group velocity of shear wave propagation, while the actual mechanical wave in a thin specimen undergoes multiple wave modes (Lamb or Rayleigh waves) based on the boundary conditions and the geometry of the medium. In the recent study using OCT with an acoustic tapping technique [48], the shear wave generated in thin tissue such as cornea showed multiple Lamb modes and was significantly influenced by various factors such as the frequency range, excitation conditions, and the ratio of the layer thickness to wavelength of the propagating wave. However, the evaluation of fixation using SWV changes does not focus on the comparison between other tissue types or processing conditions, hence, we only consider the change of group velocity of shear wave, which provides enough information of the temporal and relative change of fixation level on each specimen. For the same reason, other parallel studies using the standard measurements for hardness such as durometer, or Young's modulus from uniaxial tensile testing are not necessary for the goals of this study.

The SW-LSI measurement is vulnerable to noise from environmental factors such as room temperature and light as well as external vibrations. The room temperature was kept at 22 °C and checked in advance of the experiments. The electronic equipment and optical breadboard were mechanically isolated independently with Sorbothane (Sorbothane, Inc., Kent, OH), and the piezoelectric actuator and millifluidic chamber were also padded with Sorbothane. Thus, the noise level in the correlation images was suppressed to less than 5% regardless of shear wave excitation. In addition, the camera exposure time (50μs) was short enough to not be sensitive to changes in ambient lighting.

Our measurements with gelatin phantom and chicken breast showed good repeatability that all standard deviations (SDs) were less than 10% of the measured SWV. That error variance in mechanical property among the fresh gelatin phantoms was presumably attributed to the phantom fabrication in each individual experiment, while the heterogeneous structures (such as fat, connective tissue, and stratified layers) of the fresh chicken breast was believed to contribute to the measurement variability.

The systemic restriction of this study is the limited performance level of the experimental equipment that was borrowed from previous studies. A camera sensor with a faster frame rate and shorter exposure time than the current setting (50Hz and 50μs, respectively) may improve the sensitivity on laser speckle pattern changes. A stabilized laser source at near-infrared wavelength was unavailable, but, would be expected to avoid larger optical absorption of hemoglobin [49] and demonstrate significantly better penetration in tissues [50], [51].

Another limitation of our systems is that the shear wave was induced by physical contact with a piezo actuator.

This simple system was chosen because the local shear wave could be efficiently generated, and the SWV measurement could be achieved while the biospecimen was submerged in formalin. In the future, a remotely induced shear wave by an ultrasonic transducer [35] can be applied to develop a closed channel monitoring system which is superior in reducing manual handling requirements and allows full automation with lower risk of contamination.

Clinical Impact:

Rapid and optimal tissue fixation has been of great interest in pathology and there have been numerous attempts in clinical studies as described in the introduction. Unfortunately, formalin fixation is still not well understood or controlled to the optimal fixation level in terms of results from further tissue processing protocols; staining, sectioning, and diagnosis [27], [52], [53]. For example, in breast cancer, the ASCO/CAP Task Force recommends more than 6 hours fixation for breast cancer biomarkers, ER, PgR, and HER2 [4]. On the other hand, the recent clinical studies, with the goal of speeding up the pathology and hence breast cancer diagnosis, investigated the potential of rapid CNB fixation regarding the sensitivity of essential biomarkers. Sujoy et al. in 2014 [7] reported that no negative effect on ER-IHC with only 30 minutes fixation. And in 2017, Halilovic *et al.* [8] presented good agreement of ER, E-cadherin IHC, and HER2 fluorescence in situ hybridization (FISH) between 60-90 minutes fixation with CNB and a traditionally fixed resection. Those breast cancer clinical guidelines and studies indicate that there is a large gap between the acceptable fixation level in some pathology labs (as short as 30 minutes) and the recommended guideline. In other biomarkers tissue studies, consensus is not achieved; thus, generally described with a broad spectrum of fixation times, (e.g., 6 to 48 hours for lung cancer diagnosis [54] and 8 to 72 hours for multiplexed QD ISH assay of ERG and PTEN in prostate cancer [5]). Hence, the significant advantage of our proposed approach of real-time monitoring of fixation level may be supplemented within the streamlined protocols of tissue preparation to investigate the gray area of optimized fixation time, from 0.5 to 6 hours of sample immersion in NBF. Meanwhile, this fixation monitoring system can also offer significant improvement in quality assurance for current histopathology lab environments in which programmed overnight tissue batch processing with an automated tissue processor is common. For example, one sample of hundreds of tissue cassettes can be extracted from the tissue processor to confirm an optimal fixation level or a small set of CNBs in channels can be monitored during formalin fixation. In addition, our system is also adaptable to the use of a wide range of fixation chemicals from NBF to alcohol mixtures. Although characterizing optimal fixation levels based on the various types, sizes, and heterogeneous nature of tissue in addition to IHC staining methods requires more extensive clinical studies, it is believed that the shear wave LSI system can provide important tissue fixation information for pathologists without making compromises in their clinical timelines and protocols.

V. CONCLUSION

We demonstrated the feasibility of the LSI system to measure the change of SWV due to formalin fixation in gelatin phantom and chicken breast. To our best knowledge, the LSI system for SWV measurement in biological tissue, which is strongly scattering and even more during fixation, has not been reported. Furthermore, this is the first reported use of LSI for quantitative monitoring the formalin fixation process, which is a highly sensitive and relatively low-cost optical configuration without experimental complexity of other imaging modalities, such as ultrasound, OCT and MRI. The potential clinical importance of our system is efficiently and reproducibly controlling the gray area of formalin fixation (from the initial 0.5 to 6 hours of tissue immersion) which lays the framework for point-of-care histopathological evaluation in addition to omics biomarker analyses.

REFERENCES

[1] H. Fox, F. B. Johnson, J. Whiting, and P. P. Roller, "Formaldehyde fixation," *J. Histochem. Cytochem.*, vol. 33, no. 8, pp. 845–853, Aug. 1985.

[2] M. E. Boon, P. O. Gerrits, H. E. Moorlag, P. Nieuwenhuis, and L. P. Kok, "Formaldehyde fixation and microwave irradiation," *Histochem. J.*, vol. 20, nos. 6–7, pp. 313–322, Jun. 1988.

[3] R. Thavarajah, V. K. Mudimbaimannar, J. Elizabeth, U. K. Rao, and K. Ranganathan, "Chemical and physical basics of routine formaldehyde fixation," *J. Oral Maxillofac. Pathol.*, vol. 16, no. 3, pp. 400–405, Sep./Dec. 2012.

[4] A. C. Wolff *et al.*, "Human epidermal growth factor receptor 2 testing in breast cancer: American society of clinical oncology/college of american pathologists clinical practice guideline focused update," *Arch. Pathol. Lab Med.*, vol. 138, no. 2, pp. 241–256, Feb. 2014.

[5] U. G. Sathyanarayana *et al.*, "Determination of optimum formalin fixation duration for prostate needle biopsies for immunohistochemistry and quantum dot FISH analysis," *Appl. Immunohistochem. Mol. Morphol.*, vol. 23, no. 5, pp. 364–373, May 2015.

[6] J. A. Ibarra and L. W. Rogers, "Fixation time does not affect expression of HER2/neu: A pilot study," *Amer. J. Clin. Pathol.*, vol. 134, no. 4, pp. 594–596, Oct. 2010.

[7] V. Sujoy, M. Nadji, and A. R. Morales, "Brief formalin fixation and rapid tissue processing do not affect the sensitivity of ER immunohistochemistry of breast core biopsies," *Amer. J. Clin. Pathol.*, vol. 141, no. 4, pp. 522–526, Apr. 2014.

[8] A. Halilovic *et al.*, "Brief fixation enables same-day breast cancer diagnosis with reliable assessment of hormone receptors, E-cadherin and HER2/Neu," *J. Clin. Pathol.*, vol. 70, no. 9, pp. 781–786, Sep. 2017.

[9] A. M. Gown, "Tweaking and nudging toward improved-IHC quality," *Appl. Immunohistochem. Mol. Morphol.*, vol. 17, no. 5, pp. 363–365, Oct. 2009.

[10] N. S. Goldstein, M. Ferkowicz, E. Odish, A. Mani, and F. Hastah, "Minimum formalin fixation time for consistent estrogen receptor immunohistochemical staining of invasive breast carcinoma," *Amer. J. Clin. Pathol.*, vol. 120, no. 1, pp. 86–92, Jul. 2003.

[11] H. Yaziji and T. Barry, "Diagnostic immunohistochemistry: What can go wrong?" *Adv. Anat. Pathol.*, vol. 13, no. 5, pp. 238–246, Sep. 2006.

[12] J. D. Webster, M. A. Miller, D. Dusold, and J. Ramos-Vara, "Effects of prolonged formalin fixation on diagnostic immunohistochemistry in domestic animals," *J. Histochem. Cytochem.*, vol. 57, no. 8, pp. 753–761, Aug. 2009.

[13] L. Agrawal, K. B. Engel, S. R. Greytak, and H. M. Moore, "Understanding preanalytical variables and their effects on clinical biomarkers of oncology and immunotherapy," *Semin. Cancer Biol.*, vol. 52, pp. 26–38, Oct. 2018.

[14] S. Susman *et al.*, "The role of the pathology department in the preanalytical phase of molecular analyses," *Cancer Manag. Res.*, vol. 10, pp. 745–753, Apr. 2018.

[15] S. Farkona, E. P. Diamandis, and I. M. Blasutig, "Cancer immunotherapy: The beginning of the end of cancer?" *BMC Med.*, vol. 14, no. 1, p. 73, May 2016.

[16] K. K. Lindfors and C. J. Rosenquist, "Needle core biopsy guided with mammography: A study of cost-effectiveness," *Radiology*, vol. 190, no. 1, pp. 217–222, Jan. 1994.

[17] M. J. Silverstein *et al.*, "Image-detected breast cancer: State-of-the-art diagnosis and treatment," *J. Amer. College Surgeons*, vol. 209, no. 4, pp. 504–520, Oct. 2009.

[18] M. A. Ganott *et al.*, "Ultrasound guided core biopsy versus fine needle aspiration for evaluation of axillary lymphadenopathy in patients with breast cancer," *ISRN Oncol.*, vol. 2014, Jan. 2014, Art. no. 703160. [Online]. Available: https://www.hindawi.com/journals/isrn/2014/703160/

[19] S. Loeb, H. B. Carter, S. I. Berndt, W. Ricker, and E. M. Schaeffer, "Complications after prostate biopsy: Data from SEER-medicare," *J. Urol.*, vol. 186, no. 5, pp. 1830–1834, Nov. 2011.

[20] K. E. Calhoun and B. O. Anderson, "Needle biopsy for breast cancer diagnosis: A quality metric for breast surgical practice," *J. Clinical Oncol.*, vol. 32, no. 21, pp. 2191–2192, 2014.

[21] D. Chafin, A. Theiss, E. Roberts, G. Borlee, M. Otter, and G. S. Baird, "Rapid two-temperature formalin fixation," *PLoS One*, vol. 8, no. 1, Jan. 2013, Art. no. e54138.

[22] I. E. Chesnick, J. T. Mason, T. J. O. Leary, and C. B. Fowler, "Elevated pressure improves the rate of formalin penetration while preserving tissue morphology," *J. Cancer*, vol. 1, pp. 178–183, Oct. 2010.

[23] N. Zou *et al.*, "Ultrasound-facilitated formalin fixation of biological specimens," *Biotech. Histochem.*, vol. 86, no. 6, pp. 413–420, Dec. 2011.

[24] J. P. Bulte *et al.*, "One-day core needle biopsy in a breast clinic: 4 years experience," *Breast Cancer Res. Treat.*, vol. 137, no. 2, pp. 609–616, Jan. 2013.

[25] C. B. Moelans, D. Oostenrijk, M. J. Moons, and P. J. Van Diest, "Formaldehyde substitute fixatives: Effects on nucleic acid preservation," *J. Clin. Pathol.*, vol. 64, no. 11, pp. 960–967, Nov. 2011.

[26] F. Boissiere-Michot *et al.*, "The non-crosslinking fixative RCL2-CS100 is compatible with both pathology diagnosis and molecular analyses," *Pathol. Oncol. Res.*, vol. 19, no. 1, pp. 41–53, Jan. 2013.

[27] J. Y. Chung *et al.*, "Histomorphological and molecular assessments of the fixation times comparing formalin and ethanol-based fixatives," *J. Histochem. Cytochem.*, vol. 66, no. 2, pp. 121–135, Feb. 2018.

[28] C. Perry *et al.*, "A buffered alcohol-based fixative for histomorphologic and molecular applications," *J. Histochem. Cytochem.*, vol. 64, no. 7, pp. 425–440, Jul. 2016.

[29] R. Das, C. W. Burfeind, G. M. Kramer, and E. J. Seibel, "Pathology in a tube: Step 1. Fixing, staining, and transporting pancreatic core biopsies in a microfluidic device for 3D imaging," *Proc. SPIE*, vol. 8976, Mar. 2014, Art. no. 89760R. [Online]. Available: https://www.spiedigitallibrary.org/conference-proceedings-of-spie/8976/1/Pathology-in-a-tube--Step-1-Fixing-staining-and/10.1117/12.2041106.full

[30] R. Das, C. W. Burfeind, S. D. Lim, S. Patle, and E. J. Seibel, "Pathology in a tube step 2: Simple rapid fabrication of curved circular cross section millifluidic channels for biopsy preparation/3D imaging towards pancreatic cancer detection and diagnosis," *Proc. SPIE*, vol. 10491, Feb. 2018, Art. no. 1049118. [Online]. Available: https://www.spiedigitallibrary.org/conference-proceedings-of-spie/10491/1049118/Pathology-in-a-tube-step-2--simple-rapid-fabrication/10.1117/12.2291018.full

[31] E. J. Seibel, Q. Miao, R. L. Coe, and P. G. Reinhall, "Optical projection tomography microscopy (OPTM) for large specimen sizes," U.S. Patent 8 867 803 B2, Oct. 21, 2014.

[32] D. R. Bauer, B. Stevens, D. Chafin, A. P. Theiss, and M. Otter, "Active monitoring of formaldehyde diffusion into histological tissues with digital acoustic interferometry," *Proc SPIE*, vol. 3, no. 1, Feb. 2016, Art. no. 017002.

[33] A. P. Sarvazyan, M. W. Urban, and J. F. Greenleaf, "Acoustic waves in medical imaging and diagnostics," *Ultrasound Med. Biol.*, vol. 39, no. 7, pp. 1133–1146, Jul. 2013.

[34] K. Daoudi, A.-C. Boccara, and E. Bossy, "Detection and discrimination of optical absorption and shear stiffness at depth in tissue-mimicking phantoms by transient optoelastography," *Appl. Phys. Lett.*, vol. 94, no. 15, Apr. 2009, Art. no. 154103.

[35] D. S. Elson, R. Li, C. Dunsby, R. Eckersley, and M.-X. Tang, "Ultrasound-mediated optical tomography: A review of current methods," *Interface Focus*, vol. 1, no. 4, pp. 632–648, Jun. 2011.

[36] P.-Y. Chao and P.-C. Li, "Three-dimensional shear wave imaging based on full-field optical-sectioned laser speckle contrast imaging," in *Proc. IEEE Int. Ultrason. Symp. (IUS)*, Oct. 2015, pp. 1–3.

[37] T. J. Hall, M. Bilgen, M. F. Insana, and T. A. Krouskop, "Phantom materials for elastography," *IEEE Trans. Ultrason., Ferroelectr., Freq. Control*, vol. 44, no. 6, pp. 1355–1365, Nov. 1997.

[38] S. J. Kirkpatrick, D. D. Duncan, and E. M. Wells-Gray, "Detrimental effects of speckle-pixel size matching in laser speckle contrast imaging," *Opt. Lett.*, vol. 33, no. 24, pp. 2886–2888, Dec. 2008.

[39] M. Riccio, G. Breglio, A. Irace, and P. Spirito, "An equivalent time temperature mapping system with a 320×256pixels full-frame 100 kHz sampling rate," *Rev. Sci. Instrum.*, vol. 78, no. 10, Oct. 2007, Art. no. 106106,

[40] C. A. Carrascal, S. Chen, A. Manduca, J. F. Greenleaf, and M. W. Urban, "Improved shear wave group velocity estimation method based on spatiotemporal peak and thresholding motion search," *IEEE Trans. Ultrason., Ferroelectr., Freq. Control*, vol. 64, no. 4, pp. 660–668, Apr. 2017.

[41] Y. Cheng, S. Li, R. J. Eckersley, D. S. Elson, and M.-X. Tang, "Detecting tissue optical and mechanical properties with an ultrasound modulated optical imaging system in reflection detection geometry," *Biomed. Opt. Express*, vol. 6, no. 1, pp. 63–71, Jan. 2015.

[42] P.-Y. Chao and P.-C. Li, "Three-dimensional shear wave imaging based on full-field laser speckle contrast imaging with one-dimensional mechanical scanning," *Opt. Express*, vol. 24, no. 17, pp. 18860–18871, Aug. 2016.

[43] M. Orescanin and M. Insana, "Shear modulus estimation with vibrating needle stimulation," *IEEE Trans. Ultrason., Ferroelectr., Freq. Control*, vol. 57, no. 6, pp. 1358–1367, Jun. 2010.

[44] R. K. Manapuram *et al.*, "Estimation of shear wave velocity in gelatin phantoms utilizing PhS-SSOCT," *Laser Phys.*, vol. 22, no. 9, pp. 1439–1444, Sep. 2012.

[45] Y. Ling *et al.*, "Effects of fixation and preservation on tissue elastic properties measured by quantitative optical coherence elastography (OCE)," *J. Biomech.*, vol. 49, no. 7, pp. 1009–1015, May 2016.

[46] M. Srinivasan and D. Sedmak, "Effect of fixatives and tissue processing on the content and integrity of nucleic acids," *Amer. J. Pathol.*, vol. 161, no. 6, pp. 1961–1971, Dec. 2002.

[47] B. F. Kennedy, P. Wijesinghe, and D. D. Sampson, "The emergence of optical elastography in biomedicine," *Nature Photon.*, vol. 11, no. 4, pp. 215–221, Apr. 2017.

[48] Ł. Ambroziński *et al.*, "Acoustic micro-tapping for non-contact 4D imaging of tissue elasticity," *Sci. Rep.*, vol. 6, Dec. 2016, Art. no. .38967.

[49] S. Anand *et al.*, "Effects of formalin fixation on tissue optical properties of in-vitro brain samples," *Proc. SPIE*, vol. 9321, Mar. 2015, Art. no. 93210Z. [Online]. Available: https://www.spiedigitallibrary.org/conference-proceedings-of-spie/9321/93210Z/Effects-of-formalin-fixation-on-tissue-optical-properties-of-in/10.1117/12.2076961.full

[50] H. Zhang, D. Salo, D. M. Kim, S. Komarov, Y.-C. Tai, and M. Y. Berezin, "Penetration depth of photons in biological tissues from hyperspectral imaging in shortwave infrared in transmission and reflection geometries," *Proc SPIE*, vol. 21, no. 12, Dec. 2016, Art. no. 126006.

[51] C. Ash, M. Dubec, K. Donne, and T. Bashford, "Effect of wavelength and beam width on penetration in light-tissue interaction using computational methods," *Lasers Med. Sci.*, vol. 32, no. 8, pp. 1909–1918, Nov. 2017.

[52] M. L. Lerch, D. R. Bauer, D. Chafin, A. Theiss, M. Otter, and G. S. Baird, "Precision medicine starts with preanalytics: Real-time assessment of tissue fixation quality by ultrasound time-of-flight analysis," *Appl. Immunohistochem. Mol. Morphol.*, vol. 25, no. 3, pp. 160–167, Mar. 2016.

[53] J. M. M. Cates and K. A. Troutman, "Quality management of the immunohistochemistry laboratory: A practical guide," *Appl. Immunohistochem. Mol. Morphol.*, vol. 23, no. 7, pp. 471–480, Aug. 2015.

[54] M. Dietel *et al.*, "Diagnostic procedures for non-small-cell lung cancer (NSCLC): Recommendations of the European expert group," *Thorax*, vol. 71, no. 2, pp. 177–184, Feb. 2016.